Finite Element Simulation of Interfacial Fracture between Fe_3C and α-Fe Based on Cohesive Zone Law Deriving from Molecular Dynamics

Taolong Xu[1], Xiangguo Zeng[1], Anlin Yao[2,*], Yi Liao[1], Rongpeng Xu[1,3]

[1] College of Architecture and Environment, Sichuan University, Chengdu 610065, PR China
[2] School of Petroleum Engineering, Southwest Petroleum University, Chengdu 610500, PR China
[3] School of Engineering, Alfred University, Alfred, NY, USA 14802
* Corresponding author: yaoalt@sina.com

Abstract Once the cohesive zone model (CZM) is used to describe material behavior near crack front zone, it was convenient to simulate crack propagation by using finite element. Actually, the cohesive zone model is depicted by means of the traction-separation relation. But, It is very difficult to determinate such a relation, i. e, the traction-separation relation, through experiment, respectively. The traction-separation laws of most previous work are often assumed rather than predicted. First of all, in order to parameterize and obtain a traction-separation (T-S) law, Molecular dynamics (MD) simulations via Large-Scale Atomic/Molecular Massively Parallel Simulator (LAMMPS) are carried out at atomic scale for the deformation and fracture of *Fe_3C-α-Fe* interface in tensile loadings at different temperatures in our study. Then, the generated parameterized traction-separation law is implemented in the finite element model with the behavior of the CZM described by traction-separation (T-S) law. Finally, the ABAQUS finite element commercial software is employed to simulate the crack propagation behavior for *X70* pipeline steel CT specimen.

Keywords Crack propagation, Cohesive zone model, Molecular dynamics, Parameterized traction-separation law

1. Introduction

After more than ten years of construction and development, the length of high pressure gas pipeline made of *X70* steel has over 8,000 kilometers in China. As a structure material, *X70* pipeline has high excellent strength and toughness. The research of mechanical properties, deformation and fracture mechanism of *X70* steel become more and more important. Metallographic analysis show that *X70* steel mainly consists of ferrite and a small amount of pearlite[1]. Physics-based modeling of fracture begins at nanometer length scales in which atomic simulation is used to predict the formation, propagation and interaction of fundamental damage mechanisms[2,3]. In recent years, in this research field, great attentions have been paid to use the cohesive zone model (CZM) to set up the leaking between atomic-scale and macro-scale near crack front zone. The theory of cohesive zone model may be traced back to the early works by Dugdale[4] and Barrenblatt[5], in which both concepts of atomistic de-cohesion and the defect process zone are established. Xu and Needleman[6,7] first related the cohesive zone model (CZM) with finite element analysis, and they developed the cohesive finite element method and successfully applied it to simulate crack propagation problems. Cohesive elements that possess zero volume in an undeformed state are inserted between bulk elements. They are particularly appropriate when the crack propagation path can be well-reasoned. Cohesive zone law defines the relation between traction and crack opening displacement. Because it is difficult to direct experimentally quantify the relation, construction of such a law has been a challenging task in the past decade[8,9]. The traction-separation (T-S) relationship in a CZM is generally parameterized through empirical data, such as by using the macroscopic fracture toughness of the material or by conducting nanocrystalline experiments to obtain the stress-strain data[10]. The problem with inputting macroscopic/empirical values of fracture toughness is that these are aggregate responses of hundreds of thousands of grains applied to the location where fracture occurs[11].

This paper simulated a compact tension fracture mechanics specimen through cohesive elements whose T-S relation between *Fe_3C* and *α-Fe* was derived from MD simulations. These results enable

us to make several recommendations to improve the methodology used to derive cohesive laws from MD simulations. Furthermore the numerical analysis presented here helps to better understand the crack propagation behavior of *X70* pipeline steel.

2. MD model and simulation procedure

2.1. EAM/FS potential function

Molecular dynamics method, which considers the atomic movement is governed by Newton equations under the experience potential field which was determined by all other atoms in multi-body system, can be used to calculate system dynamic problems consisting of a large number of atoms. The interaction between the atoms can be reflected through potential function. Proper selection of the potential function types as well as the potential function parameters plays the key roles in the simulation results.

As a representative of the multi-body potential, the basic idea of Embedded Atom Method (EAM) is to divide the total potential energy into pair potential among the interaction of atomic crystal and the embedded potential of nucleus, which are embedded in the electron cloud and representing the interaction of multi-body.

In 1984, based on EAM potential, Finnis and Sinclair[12] developed a kind of multi-body potential with embedded energy function, hereinafter referred to as the FS-EAM potential. Like the majority of the potential functions based on EAM potential, the FS-EAM potential can be used to simulate the atomic-scale mechanisms of deformation and failure in metal materials, and the i_{th} atom potential energy can be expressed by the equation:

$$E_i = F_\alpha \sum_{j \neq i} \rho_{\alpha\beta}\left(r_{ij}\right) + \frac{1}{2}\sum_{j \neq i} \phi_{\alpha\beta}\left(r_{ij}\right) \tag{1}$$

The form of EAM potential and FS-EAM potential is consistent, but the ρ is the function of the type of atom i and j, which means the contribution of different elements on the same position of the atoms of the total electron density is not equal, and it can be given by the following expression:

$$\rho_i = \sum_{j \neq i} \rho_j\left(r_{ij}\right) \tag{2}$$

In expression (2),

$$\rho_j\left(r_{ij}\right) = \sum_{k=1}^{2} A_k \left(R_k - r_{ij}\right)^3 H\left(R_k - r_{ij}\right) \tag{3}$$

$$\phi_{ij}\left(r_{ij}\right) = \sum_{k=1}^{6} a_k \left(r_k - r_{ij}\right)^3 H\left(r_k - r_{ij}\right) \tag{4}$$

Thereinto,

$$H\left(x\right) = \begin{cases} 0 & \left(x > 0\right) \\ 1 & \left(x < 0\right) \end{cases} \tag{5}$$

In which, A_k, R_k, a_k, r_k for constants, and $R_1 > R_2$, $r_1 > r_2 > \ldots > r_6$.

The melting point of *α-Fe* was obtained by LAMMPS in order to verify the FS-EAM potential. The initial configuration of the simulated system was composed of 8×8×5 *bcc-Fe* cellular, a total of 640 atoms, the time step was 0.005*ps*, using three-dimensional periodic boundary conditions, let the system in the 2.5*K* relaxation 100000 steps, and then use the Nose-Hover method to keep the pressure around zero, and then elevated system temperature from T=2.5*K* to 2500*K* the rate of 4.1625×1011*K/s*. During the simulation, the thermodynamic results were output every 1000 steps, as shown in Fig.1 and Fig.2, respectively. The average atomic volume almost linear increase with

the temperature and simulation time in the heating process, which turn upsuddenly increases when the temperature reaches a certain value. This phenomenon indicated that the system had undergone some kind of phase transition. The melting point of *α-Fe* is about 1873*K*, and simulations in the 1990*K* near a phase transition, increased by 6.2% than its equilibrium melting point. Such deviation derived from the melting point between the MD simulation and the actual sample were relatively common, which was related with using three-dimensional periodic boundary conditions in simulation system, the limited number of particles and the accuracy of interaction potential.

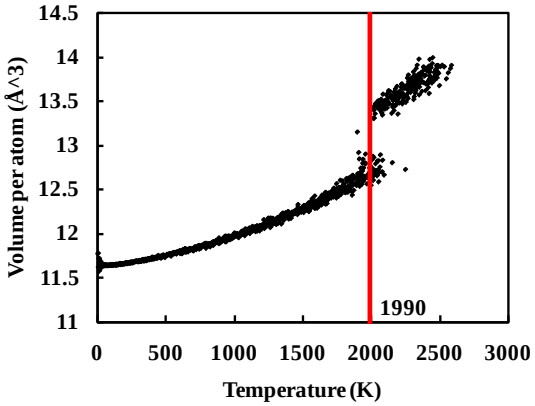

Figure 1. The mean volume of single atom changing with temperature during heating process

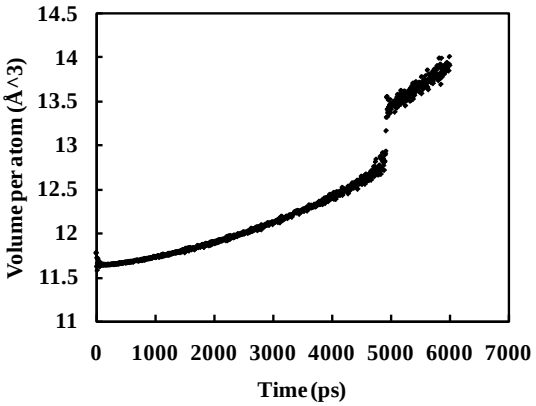

Figure 2. The mean volume of single atom changing with modeling time during heating process

In the simulation, the system contains two elements, i.e., *Fe* and *C* .The *Fe*/*C* alloy EAM/FS potential function parameters[13], which were evaluated by melting point testing were adopted in this work.

2.2. Specimen setup

The MD model used for conducting fracture studies is shown in Fig. 3. The dimensions in the x-y plane are 200*Å*×192*Å* with thickness in the z-direction equaling 8.82*Å*.The total atoms of the model were 31978. The x y z coordinate system represents the lattice directions [0 1 0], [1 0 0] and [0 0 1] respectively. In the model free boundary conditions were used in the x- and y-directions, while it was periodic boundary in the z-direction. As shown in Fig. 3, the simulation domain is divided into three regions. Atoms that are in regions 1 and 3 are boundary atoms through which tensile load are applied. A crack of length 100*Å* was generated at the interface of Fe_3C and *α-Fe*. During MD simulations of tensile crack propagation, the system is uniformly stretched (by moving each atom a distance corresponding to a uniform normal strain increment) in the Y-direction at each time step[2]. And the duration was less than 0.001*ps*, which made it relax freely till the valley of energy status. Molecular dynamics simulation time step was given with t=0.001*ps*. Integral calculation on system movement equation through Verlet techniques was applied during simulation. The simulation process: applying *NVE* system tracking and in every time step, maintain the temperature (300*K*, 473*K* and 673*K*) constantly through re-calibration of the speed of atoms. Firstly perform static relaxation to bring the system to the minimum energy status, and applying 3.128*Å*/*ps* strain rate in *y* direction. A systematic analysis on the effect of strain rate was not conducted in this study.

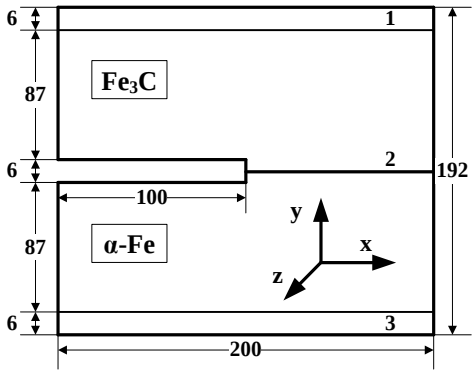

Figure 3. The molecular dynamics models with pre-existing crack along the interface, all dimensions are in *Å*

Due to the complex crystal structure of *Fe_3C*, in this paper, only [110] orientation faces were simulated, as shown in Fig.4. In Fig.4(a), for cementite (*Fe_3C*) with complex trapezius crystal structure, every single cell contains 4 carbon atoms (gray ball) and 12 Fe atoms (blue ball)[14], while Fig.4(b) shows that the interface structure combined with body-centered cubic iron and cementite.

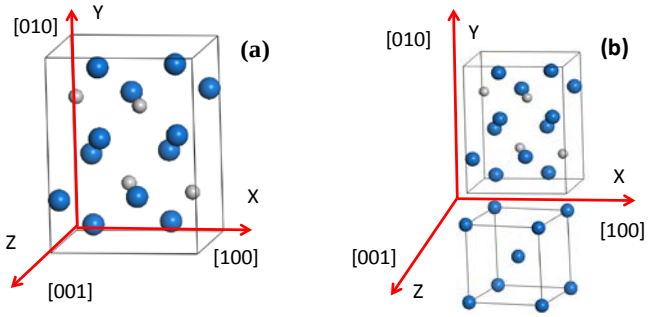

Figure 4. *Fe_3C* unit cell and interface structure schematic drawing

3. Simulation results

3.1. Stress-strain response

Fig.5 shows the atomic snapshots of tensile mode failure at temperature of 473*K* in different strains. The simulation model starts with elastic deformation from its initial state (Fig. 5(a)) to the yield stress at a strain ε= 0.0303. On yielding there is large scale debonding along the *Fe_3C-Fe* interface (Fig. 5(b)). After this the *Fe_3C-Fe* interface progressively degrades (Fig. 5(c)) and carries virtually no load at strain values above 0.1106.

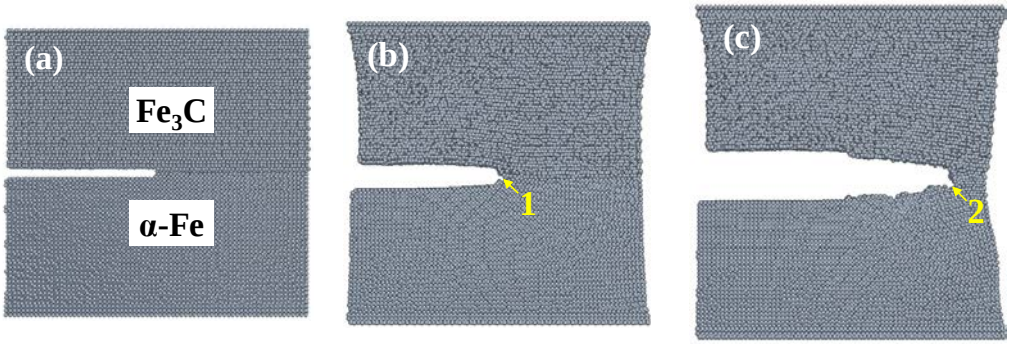

Figure 5. MD snapshots of tensile mode failure of a cracked interface at 473*K* at strains (ε) of (a) ε= 0.00, (b) ε=0.0397 and (c) ε= 0.0960. Areas of interest are (1) crack initiation and (2) crack progression

Selected examples were examined to characterize stress-strain curves dynamics. Average atomic

stresses based on the Virial theorem[16] were used to estimate global normal (*yy*) stresses applied to the system, which could be defined as the volume average of potential for all of the atoms in the system:

$$\sigma_{ij} = \frac{1}{V_i}\left[\frac{1}{2}\sum_{j\neq i}^{N} r_{ij} \otimes f_{ij}\right] \tag{6}$$

Zhou[15] has presented the specific formula for calculation:

$$\sigma_{ij} = \frac{1}{V}\left[\frac{1}{2}\sum_{\alpha,\beta}^{N}\left(-\frac{1}{r}\frac{\partial\phi}{\partial r}\right) r_i r_j \,\middle|\, r = r_{\alpha\beta}\right] \tag{7}$$

The strain used here is the nominal strain actually. The results were used to map the stress-strain curves. To reduce thermal oscillation, values of stress and strain were averaged over 10 time steps (each time step is 0.001*ps*). A short averaging time of 0.01*ps* was used to retain the time dependence of the properties. While this averaging time is small, it still helps mitigate thermal noises as the averaging is performed over many atoms. The normal stress-normal strain curve obtained from the tensile mode simulation is shown in Fig. 6. It indicates that during the tensile test, the normal stress initially linearly increases as the normal strain is increased, corresponding to an elastic deformation of the system. To examine the effect of the presence of the crack, a similar normal stress-normal strain curve obtained from the tensile mode loading of with a crack sample is included in Fig.7, the maximum normal stress at same temperature is significantly reduced and only about half value of the no crack model.

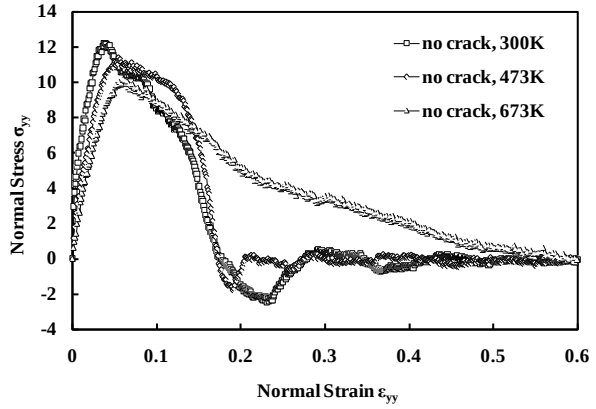

Figure 6. The normal stress-normal strain curve of models without crack at different temperatures

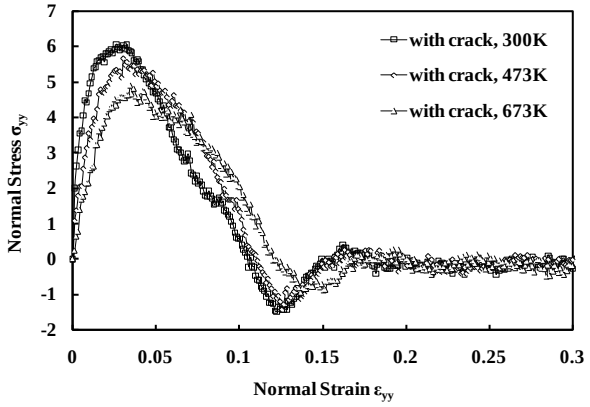

Figure 7. The normal stress-normal strain curve of models with cracks at different temperatures

The simulation results for the elastic modulus and maximum stress as a function of the simulated temperature for both with and without crack models are summarized in Table 1. They have the same changing regularity for both perfect interface and imperfect interface, which is found the elastic modulus and maximum stress are reduced by the increase of simulated temperature, and the maximum values of modulus and maximum stress for no crack model at roomtemperature are seen to be 332.67*GPa* and 12.17*GPa*, respectively. Presence of a crack reduces the maximum load carrying capacity and additionally reduces the stiffness of the composite system.

Table 1. simulation results of model failure.

Crack	Simulated temperature (*K*)	Modulus (*GPa*)	Maximum stress (*GPa*)
No	300	332.67	12.17
	473	210.11	11.40
	673	193.18	9.88
Yes	300	186.94	6.04

473	187.41	5.67
673	142.42	4.90

3.2. Traction-separation response

To quantify the cohesive zone law, stresses and displacements at local positions are analyzed in detail. MD simulations are conducted for temperatures of 300*K*, 473K and 673*K* for tensile mode failure to develop traction-separation relationships for the CZM. Tensile (σ_{yy}) tractions are calculated as the average atomic stresses at a region of $20\text{Å}\times 10\text{Å}\times 8.82\text{Å}$ adjacent to the crack. As these stresses are calculated locally near the crack surface they therefore relate to the traction in the traction–separation law [17].The average traction and opening displacement associated with region were calculated using all the points in the region adjacent to the crack. This effectively reduces the scatter of the data [9].

Regardless of the temperature of the system or the mode of failure, the traction always initially increases as the crack opening distance was increased until they reached a peak value. The traction then decreased as the crack opening was further increased. To represent the CZM, a model that includes an exponential term is suggested to approximate the traction-separation responses shown in Fig. 8 for tensile mode failure. It indicates that the stresses initially increased as the crack opening distance was increased until they reached a peak value. The result for the maximum stress as a function of the simulated temperature is summarized in Table 2.

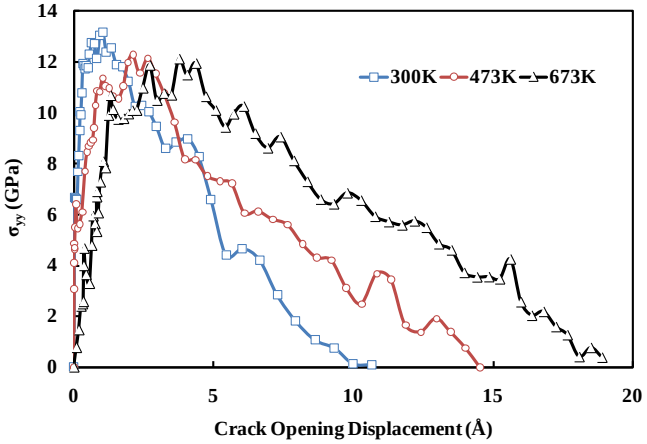

Figure 8. Traction-Separation relationship for tensile mode failure in a Fe_3C-*Fe* interface

Table 2. Simulation results to gage the effect of temperature CZM

Case	Simulated temperature (*K*)	Maximum stress (*GPa*)
1	300	13.15
2	473	12.29
3	673	12.11

4. Parameterization of the T-S law

Researches constructed cohesive models as that: tractions increase until reach a maximum, and then approach zero when the separation displacement increases. The thickness of the interface in the unloaded state is considered as zero. Tvergaard and Hutchinson (1993) [18] introduced traction-separation relation: let δ_n^c and δ_t^c be the maximum allowable normal and tangential components of the cohesive element. δ_n and δ_t denote the normal and tangential components of the relative displacement of the crack faces across the interface in the zone where the fracture

processes are occurring (as shown in Fig.9). The non-dimensional parameter λ is expressed by Eq.(8).

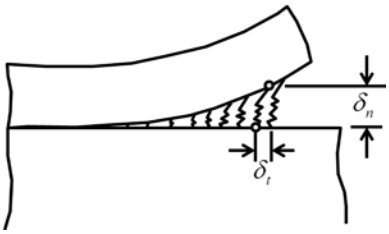

Figure 9. Traction-separation relation

$$\lambda = \left\{ \left(\delta_n / \delta_n^c \right)^2 + \left(\delta_t / \delta_t^c \right)^2 \right\}^{1/2} \tag{8}$$

Failure is attained in the cohesive element when λ=1.
The potential is:

$$\Pi(\delta_n, \delta_t) = \delta_n^c \int_0^\lambda \sigma(\lambda') d\lambda' \tag{9}$$

The normal and tangential components of the traction are given by:

$$\begin{aligned} T_n &= \frac{\partial \Pi}{\partial \delta_n} = \frac{\sigma(\lambda)}{\lambda} \frac{\delta_n}{\delta_n^c} \\ T_t &= \frac{\partial \Pi}{\partial \delta_t} = \frac{\sigma(\lambda)}{\lambda} \frac{\delta_t}{\delta_t^c} \frac{\delta_n^c}{\delta_t^c} \end{aligned} \tag{10}$$

If the tangential component of the traction is zero, the traction-separation law is a purely normal separation. The peak normal traction under purely normal separation is termed the interface strength. Generally, for Mode I cohesive zone model it only contains opening mode fracture, the relationship between the cohesive traction and the separation displacement could be expressed as:

$$F(\lambda) = \sigma = \sigma_c f(\lambda) \tag{11}$$

In this equation, σ_c is the peak traction, f is a dimensionless function which relate to the shape of the cohesive traction-separation displacement curve.
A relationship between the traction and the crack opening displacement must be obtained when we use cohesive element. In the CZM, the fracture process zone is simplified as being an initially zero-thickness zone, composed of two coinciding surfaces. Under loading, the two surfaces separate and the traction between them varies in accordance with a specified T-S law. In our study a parameterized exponential T-S law is proposed based on the MD simulations. According to Eq.(11), the traction-separation law ($F(\lambda)$) is then implemented through Eq.(12). In Eq.(12) the maximum cohesive strength (σ_c) is simulated at room temperature. The constants parameterized from the MD results of Mode I are obtained in table 3. According to Eq.(12) and table 3, the curve of traction-separation relationships under different simulate temperatures has shown in Fig.10.

$$F(\lambda) = \sigma_c f(\lambda) = A\sigma_c \lambda \exp(-B\lambda) \times (1 - 0.001T) \tag{12}$$

Table 3The constants parameterized from the MD results of Mode I.

Simulated temperature (*K*)	Maximum stress (*GPa*)	*A*	*B*
300	13.15	2.6338	0.8142
473	12.29	1.6951	0.4712
673	12.11	1.1905	0.2643

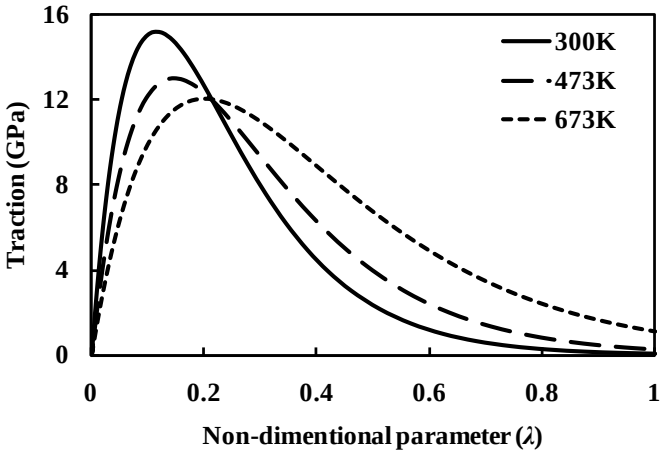

Figure 10. Traction-separation relationships under different simulate temperatures

5. Simulation of the T-S fracture test

In order to model stable crack growth under static loading and analyze cohesive behavior derived from MD towards greater length scales, it is necessary to examine a scenario in which the effective stress intensity factor in the process of crack growth. Thus, we perform a simulation of crack growth for a CT specimen subject to displacement loading via prescribed motion of loading pins. Fracture of a CT specimen can verify whether the cohesive law derived from MD simulations displays behavior consistent with linear elastic fracture mechanics. The geometry and mesh of our CT specimen is shown in Fig.11. The specimen is 384 *nm* wide by H = 369 *nm* tall, with an effective width (the distance between the pin holes and the uncracked edge) of W = 307 *nm*, an initial crack length of a = 155 *nm* ($a/W \approx 0.5$), and pin holes of radius 38.4 *nm*. Our initial geometry contains a zero-width crack rather than the finite-width crack. Cohesive elements are placed along the predefined crack path, and are 1*Å* wide. This element size enables the cohesive zone to be resolved over a length of approximately 45*Å* (45 elements).The parameterized T-S law given was implemented in ABAQUS to simulate the behavior of the CZM. For the FE model of outside of the CZM, two-dimensional continuum plane strain incompatible elements (CPEI4) were used with isotropic material properties to represent the bulk elastic behavior while two-dimensional cohesive elements (COH2D4) were used for the CZM.

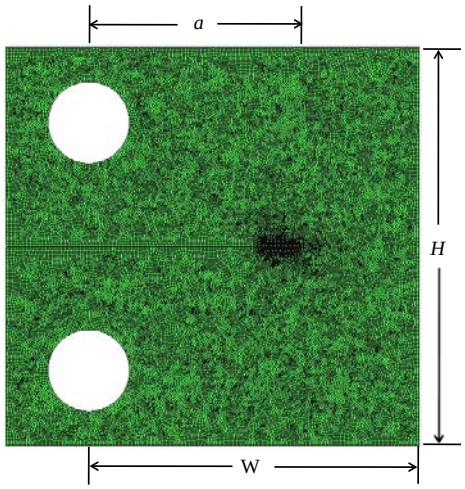

Figure 11. FEA mesh of CT specimen. The specimen's height H=369 *nm*, its effective width W=307 *nm*, and its initial crack length a=155 *nm*

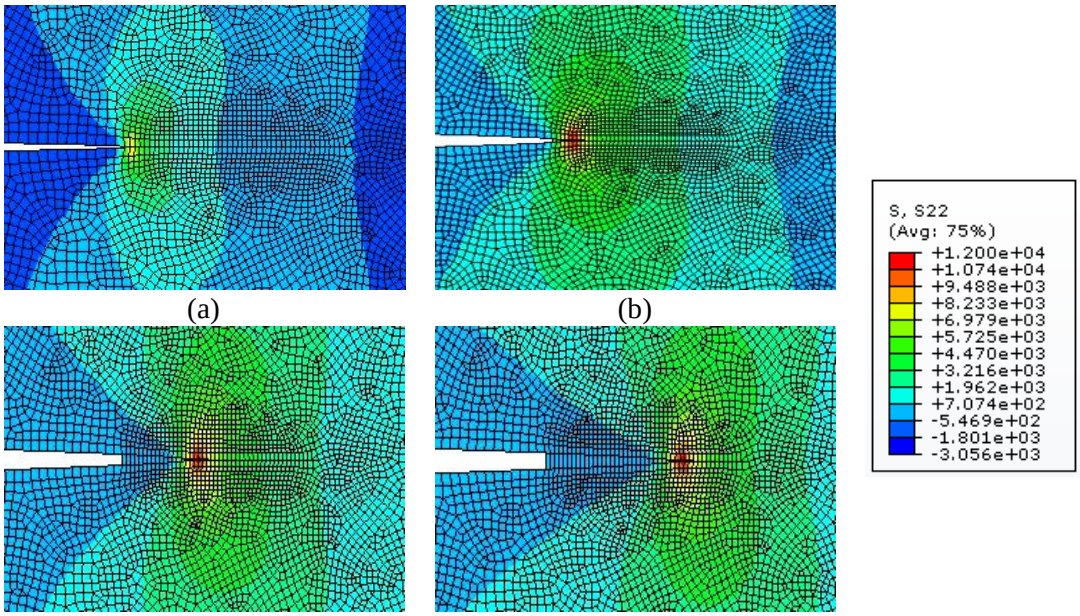

Figure 12. Static crack growth in the CT geometry. Loading–pin displacements of (a) 24Å, (b) 40Å, (c) 60Å, and (d) 70Å are shown. Plots are colored according to element values of σ_{yy} in units of *GPa* as shown in the legend

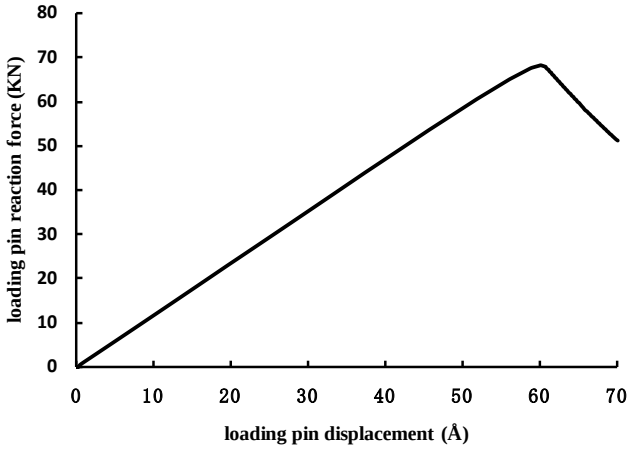

Figure 13. Reaction force versus loading-pin displacement for CT specimen

The crack opening behavior due to displacement of the top and bottom pins is observed in Fig.12. Before crack propagation begins to occur, the cohesive zone begins to form, as seen in Fig.12(a) and (b). Once a critical displacement is reached, crack propagation is seen in Fig.12(c) and (d).

We can further verify our analysis by taking the value of peak load in Fig.13, 68.06 *kN*, and combining it with geometric dimensions of the system to obtain the stress intensity factor. We obtain a value for fracture toughness of J_c=0.42 *MPa·m*. This value lies close to experimental result in literature [19].

Our study shows that the estimated fracture toughness coincides with test value from experiment. It shows the expected linear relationship between loading-pin displacement and reaction force. More complex fracture mechanics problems can be analyzed through combining the cohesive law derived from MD simulations and finite element method.

6. Conclusion

(1) Molecular dynamics simulations under a special configuration have been performed to study the mechanism of Fe_3C-Fe interface under Mode I loading condition at different temperatures, and the FS-EAM potential used in LAMMPS is certified by melting point verification.
(2) The elastic modulus and maximum stress as a function of the simulated temperature for both with and without crack models, and the maximum values of modulus and maximum stress for no crack model at roomtemperature are seen to be 332.67*GPa*, 12.17*GPa*, 86.94*GPa* and 6.04GPa for crack model. The traction-separation relation of *X70* pipeline steel with crack is characterized by MD simulations, the peak traction value of 13.15*GPa* for tensile model at room temperature.
(3) The parameterized cohesive traction-separation relation for Mode I failure at room temperature to simulate the crack propagation behavior of *X70* pipeline steel in a FEA. The curve obtained through our simulation is agreement with predictions from linear elastic fracture mechanics, showing the expected linear relationship between loading-pin displacement and reaction force.
(4) The fracture toughness gained from our simulations is close to the experimental result. It shows our methodology is feasible. Our study may provide several novel ideas for simulating complex fracture problems based cohesive laws used in FE analysis.

Acknowledgements

Project supported by the Fundamental Research Funds for the Central Universities (Grant No. 2010SCU21014) and the Project of West-East Gas Pipeline Company at PetroChina Company Limited (Grant No. XQSGL01423).

References

[1] Yu. Ivanisenko, I. MacLaren, X. Sauvage, R.Z. Valiev,. H.J. Fecht, Shear-induced transformation in nanoscale Fe–C composite. Acta Mater., 54 (2006) 1659–1669.
[2] C.R. Dandekar, Y.C. Shin, Molecular dynamics based cohesive zone law for describing Al-SiC interface mechanics. Composites: Part A, 42 (2011) 355–363.
[3] V.Yamakova, E. Saether, D.R. Phillipsc, E.H. Glaessgen, Molecular-dynamics simulation-based cohesive zone representation of intergranular fracture processes in aluminum. Journal of the Mechanics and Physics of Solids, 54 (2006) 1899–1928.
[4] D.S. Dugdale, Yielding of steel sheets containing slits. J. Mech. Phys. Solids, 8 (1960) 100–104.
[5] G.I. Barrenblatt, The mathematical theory of equilibrium of cracks in brittle fracture. Adv. Appl. Mech., 7 (1962) 55–129.
[6] X.P. Xu, A. Needleman, Numerical simulations of fast crack growth in brittle solids. J. Mech. Phys. Solids, 42 (1994) 1397–1434.
[7] X.W. Zeng, S.F. Li, A multiscale cohesive zone model and simulations of fractures. Comput. Methods Appl. Mech. Engrg., 199 (2010) 547–556.
[8] X.W. Zhou, J.A. Zimmerman, E.D. Reedy, N.R. Moody, Molecular dynamics simulation based cohesive surface representation of mixed mode fracture. Mechanics of Materials, 40 (2008) 832–845.
[9] X.W. Zhou, N.R. Moody, R.E. Jonesa, J.A. Zimmermana, E.D. Reedyc, Molecular-dynamics-based cohesive zone law for brittle interfacial fracture under mixed loading conditions: Effects of elastic constant mismatch. Acta Materialia, 57 (2009) 4671–4686.
[10] Y.J. Wei, L. Anand, Grain-boundary sliding and separation in polycrystalline metals:application to nanocrystalline fcc metals. J Mech Phys Solids, 52 (2004) 2587–616.
[11] J.T. Lloyd, J.A. Zimmerman, R.E. Jones, X.W. Zhou, D.L. McDowell, Finite element analysis of an atomistically derived cohesive model for brittle fracture. Modelling Simul. Mater. Sci. Eng., 19 (2011) 065007.
[12] M.W. Finnis，J.E. Sinclair, A simple empirical N-body potential for transition metals. Phil.

Mag. A, 50 (1984) 45–55.
[13] D.J. Hepburn, G.J. Ackland, Metallic-covalent interatomic potential for carbon in iron, Phys. Rev. B, 78 (2008) 165115.
[14] C.W. Chiou, Jr., E.A. Carter, Structure and stability of Fe_3C-cementite surfaces from first principles. Surface Science, 530 (2003) 87–95.
[15] J.A. Zimmerman, E.B. Webb III, J.J. Hoyt, R.E. Jones, P.A. Klein, D.J. Bammann, Evaluation of continuum stress in atomistic simulation. Computational Fluid and Solid Mechanics, (2003) 804–807.
[16] M. Zhou, A new look at the atomic level virial stress: on continuum-molecular system equivalence. Proc. R. Soc. Lond. A, 459 (2003) 2347–2392.
[17] K. Gall, M.F. Hostemeyer, M.V. Schilfgaarde, M.I. Baskes, Atomistic simulations on the tensile debonding of an aluminum–silicon interface. J Mech Phys Solids, 48 (2000) 2183–212.
[18] V. Tvergaard, J.W. Hutchinson. The influence of plasticity on mixed mode interface toughness, J. Mech. Phys. Solids, 41 (1993) 1119–1135.
[19] Y.R. Feng, Y.N. Liu. Dynamic fracture of pipeline steel X70, The papers of West-East Gas Pipeline and the steel pipe application infrastructure and research technical, Petroleum Industry Press, Beijing, 2004, pp. 140–151.